REY-20
ASTANA 2019

MANUSCRIPT LENGTH ESTIMATE

Beam Interactions with Materials and Atoms
Nuclear Instruments and Methods in Physics Research, Section B.

Title of Paper : **Raman Scattering In Diamond Irradiated With High-Energy Xenon Ions**

Corresponding Author : **Nikita S. Kirilkin**

Manuscript Length Estimation Table

Number of characters[1)] (using "character count")	**30676**	**= A**
Number of 1-column tables or figures[2)]	**2**	**= B**
Number of 2-column tables or figures[2)]	**4**	**= C**

Estimated number of printed pages = (A + 1300B + 5000C)/8500	**7**

[1)] Including title, abstract, captions and references, including spaces.
[2)] Each independent figure including Fig.a, Fig.b, Fig.c, etc. must be counted separately.

RAMAN SCATTERING IN DIAMOND IRRADIATED WITH HIGH-ENERGY XENON IONS

N. M. Kazuchits[1], O. V. Korolik[1], M. S. Rusetsky[1], V. N. Kazuchits[1*], N.S. Kirilkin[2*], V. A. Skuratov[2,3,4]

[1]Belarusian State University, Minsk, Belarus,

[2]Flerov Laboratory of Nuclear Research, Joint Institute for Nuclear Research, Dubna, Russia

[3] National Research Nuclear University MEPhI, Moscow, Russia

[4]Dubna State University, Dubna, Russia

Abstract. Accumulation of radiation damage and associated mechanical stresses in diamonds irradiated with 167 MeV Xe ions to fluences $1.0\times10^{10} \div 8.15\times10^{14}$ cm^{-2} have been studied using confocal Raman spectroscopy. The spectra were measured in a backscattering geometry across the irradiated layer by scanning the edge of single crystalline synthetic samples with nitrogen concentration 3÷5 ppm. All spectra were recorded at room temperature. Parameters of the 1332 cm^{-1} first-order Raman line – the FWHM and peak position, studied as function of Xe ion fluence, were used to characterize the structural disorder and mechanical stress level.

Key words: diamond, ion implantation, radiation-induced defects, amorphization, stress, Raman scattering

* Corresponding author: N.S. Kirilkin (kirilkin@jinr.ru)

1. Introduction

Raman excitation in diamond is usually accompanied by photoluminescence (PL) and both Raman and PL spectra parameters are very sensitive to structural damage [1,2]. For instance, critical dose of amorphization of ion irradiated diamond can be estimated by due to appearance of 1530 cm^{-1} broad band [1,3–5]. Raman scattering on vibrations of intrinsic defects at 1490 and 1630 cm^{-1} provides information on vacancy and interstitial defects, respectively [1,4]. Highly sensitive PL methods can distinguish individual impurity and defect centers [2,6], that can be used to get impurity/defect distribution in the irradiated layer [7]. As known, any radiation damage of diamond lattice leads to its swelling [8–14]. Structural disorder induced by low energy ions (tens to hundreds keV) is localized near the surface. The boundary between the damaged layer and the undamaged part of the crystal is mechanically strained. For the high energy implantation (tens to hundreds MeV) the boundary of damaged layer is located beyond tens of micrometres from the surface due to radiation damage produced in elastic collisions in the end of the ion range. Crystal lattice, in this case, is inhomogeneously expanded and strained along ion range. Earlier studies of the depth distribution of impurities/defects in diamond crystals irradiated by high energy ions [7] were done using precision removal of thin layers of superhard material and utilizing PL the technique with fixed excitation and registration parameters [15]. Modern micro Raman spectrometers, combined with a 3D scanning confocal microscope and equipped with several laser excitation sources, allow performing such work at the new level. The aim of this work is depth profiling of radiation damage and mechanical stresses in diamond, irradiated with 167 MeV Xe ions.

2. Experimental

The samples used in this research were a few millimetre size plates cut along the (100) plane from single crystal type Ib synthetic diamonds produced by “AdamasInvest”, Belarus by High Pressure High Temperature (HPHT) method [16]. After mechanical polishing of both sides the thickness of the specimen was about 800 μm. Average concentration of nitrogen in the diamonds plates was calculated from visible and UV absorption spectra [16]. Visible and

UV absorption spectra were measured at room temperature in spectral range 200–900 nm using spectrometer Cary 300 Bio (Agilent Technologies). The size of the measured areas was about 0.6 mm in diameter.

Irradiation with 167MeV Xe ions was carried out at room temperature to fluences in the range 1.0×10^{10} – 8.15×10^{14} cm^{-2} at the IC-100 FLNR, JINR cyclotron [17]. After getting of definite fluence, the specimen was taken out from the irradiation module and one fourths of it was screened by a thick copper tape. Thus, four areas with different ion fluences were created on one diamond plate.

Raman spectra were registered using a micro Raman spectrometer Nanofinder High End (LOTIS TII Japan-Belarus) combined with a 3D scanning confocal microscope. Spectral resolution of the spectrometer was 2.3 cm^{-1} and 0.77 cm^{-1} for 600 lines/mm and 1800 lines/mm gratings correspondingly. Maximum spectral resolution of 0.25 cm^{-1} was reached with Echelle grating (75 lines/mm). Excitation was provided by blue (473 nm) and green (532 nm) lasers with powers of 4 and 10 mW respectively and a spot size of 1 μm. Raman spectra were gathered using a backscattering setup in the range 50-5700 cm^{-1}.

A schematic view of the experimental setup is shown in Fig.1a. A photo of a polished cross-section of the diamond plate for the fluence 8.15×10^{14} cm^{-2} with a focal point of a green laser is shown in Fig.1b. Raman spectra were registered on polished diamond cross-sections along ion trajectory (along X axis) by scanning sample with a deepening of the excitation region (Z coordinate) by 1.5 or 5.0 μm. Scanning was started beyond the sample at a distance of about 5 μm from the edge. The mid-point of the rising curve of the main Raman line intensity was chosen as the origin of the X-coordinate. Scanning step was 0.5 or 1 μm. Exposure time varied from 10 to 60 seconds and depended on the Raman signal intensity. Regions with low nitrogen concentration (3-5 ppm) were selected for examination. Such cross section geometry guaranteed the measurement of Raman spectra in the irradiated layer, corresponding to the level of damage at a selected depth and provided a higher spatial resolution.

Energy loss and depth profiles of carbon vacancies and implanted Xe ions were calculated using Monte Carlo method [18] with SRIM 2000 software [19]. Calculation results are shown in Fig.2. For 167 MeV Xe, the projected ion range in diamond is R_p = 10.67 μm with 0.44 μm straggling. Carbon vacancy concentration calculated for single ion varied from 2.24×10^6 cm^{-3} at the surface region to 6.66×10^7 cm^{-3} at the area of maximum defects creation (at the depth of 10.45 μm). According to calculations no vacancies were created beyond the projected ion range at the depth more than 11 μm.

3. Results and discussion

The Raman spectrum of the virgin diamond specimen has a narrow band at 1332 cm^{-1} originated from single-phonon light scattering and well defined two-phonon scattering band in the range from 2200 to 2660 cm^{-1}. The full width at half maximum (FWHM) of the main line was about 1.6 cm^{-1}. This value of the Raman line width is typical for structurally perfect type IIa diamonds [20–23].

The evolution of the Raman/PL spectra in the surface layer with increasing ion fluence is shown in Fig. 3. Noticeable changes occurred after the fluence more than 1×10^{11} cm^{-2}. The intensity of the main Raman line decreased, narrow lines at 3530 cm^{-1}, 3120 cm^{-1}, 1635 cm^{-1}, 1425 cm^{-1} and wide bands in the vicinity of 1230 cm^{-1} and 400 cm^{-1} appeared. The intensity of lines peaked at 3530 cm^{-1}, 3120 cm^{-1}, 1425 cm^{-1} initially increased (approximately up to a fluence 6×10^{13} cm^{-2}), and then decreased with increasing fluence. The intensity of broad bands 1220 cm^{-1} and 400 cm^{-1} and a narrow line 1635 cm^{-1} grew monotonically. At fluence 6×10^{13} cm^{-2} in the vicinity of the 1635 cm^{-1} line, Raman/PL spectrum changed and a characteristic series of narrow lines in the region of 1400-1900 cm^{-1} appeared.

Narrow lines at 3530 cm^{-1} (743 nm), 3120 cm^{-1} (638 nm), и 1425 cm^{-1} (575 nm) are ascribed to radiative recombination [2]. The 743 nm line (PL center GR1) is associated with vacancies in a neutral charge state. The lines 638 nm (PL center NV^-) and 575 nm (PL center

NV^0) are associated with the nitrogen – vacancy complex in the negatively charged and neutral charge states, respectively.

Wide bands in the vicinity of 400 cm^{-1} and 1230 cm^{-1} and series of narrow lines in the area of 1400-1900 cm^{-1} refers to Raman scattering in diamond. Wide bands at 400 cm^{-1} and 1230 cm^{-1} were observed in Raman spectra of diamonds irradiated by ions [3,4,24–26] and neutrons [26,27]. It is assumed that they are associated with amorphous sp^3 bonded carbon clusters along the ion tracks i.e. clusters of carbon displaying short-range sp^3 ordering without any long range order. These clusters are localized under high pressure inside the substantially intact diamond matrix and, therefore, are not transformed into sp^2-bonded carbon structure. Series of narrow lines in the spectral region 1400–1900 cm^{-1} was associated with Raman scattering on intrinsic point defects in a disordered by irradiation diamond lattice [28]. The most intense lines at 1500 and 1635 cm^{-1} are related [1,3,4], respectively, to vacancies and intrinsic interstitials. The peak positions of these lines shift to lower wavenumbers and FWHM are increased almost linearly with increasing damage [4].

The evolution of Raman spectra with depth in the irradiated layer is shown in Fig. 4a and 4b for two Xe ion fluences. As can be clearly seen that for 6.1×10^{12} cm^{-2}, the intensity of the radiation induced PL centers GR1, NV^-, NV^0 decreased with depth, demonstrating correlation with nuclear stopping profile. The PL bands due to complex defects NV^-, NV^0 completely disappeared at a depth of about 8 μm, while the simple vacancy center GR1 was registered up to the end of ion range. Intrinsic interstitial related Raman line at 1635 cm^{-1} had the similar behavior - both GR1 and 1635cm^{-1} lines were observed up to a depth of 10.5 μm. The intensity of the broad Raman bands at 400 cm^{-1} and 1230 cm^{-1} increased from the surface into the depth of the irradiated layer synchronously with the growth of radiation damage concentration. Raman/PL spectra beyond the ion range reverted to their initial state before irradiation and composed of the only main Raman line 1332 cm^{-1}.

For the fluence 8.15×10^{14}cm^{-2} PL was substantially suppressed even in the near surface layer (see Fig.3), therefore, the evolution of the spectra shown in Fig. 4b was due to Raman scattering. The increase of radiation damage in the diamond lattice with depth caused a decrease in intensity, broadening and low frequency shift of all Raman lines. At the region of the maximum disorder of diamond lattice (at a depth of about 9-10 μm), the main Raman line 1332 cm^{-1} disappeared. The spectrum consisted only of broad bands at 400 cm^{-1} and 1220 cm^{-1}, associated with amorphous carbon clusters, and a wide band appeared at 1530 cm^{-1} (Fig. 4b). A low-intensity line at 1635 cm^{-1} from interstitial carbon was registered on the high-frequency wing of the 1530 cm^{-1} band. The first appearance of the 1530 cm^{-1} band in the Raman spectra corresponded to fluence of 3.55×10^{14} cm^{-2} when it was registered in the damage peak region. All Raman bands ascribed to radiation defects disappeared at a depth more than 10 μm and the only scattering from the intact diamond crystal lattice is detected (1332 cm^{-1} line).

The 1530 cm^{-1} band was observed in diamonds irradiated with different ions [1,3–5,9,14,29–31]. Its appearance was associated with the critical density of radiation damage in diamond, above which the graphitization of the damaged layer occurred during annealing [32]. Spectral position and shape of the 1530 cm^{-1} band coincided with those of highly disordered by ion irradiation graphite sp^2 layers [1,5,33–35]. The formation of amorphous, not graphite, carbon as a result of irradiation of diamond with heavy ions was confirmed by direct measurements of electron diffraction [36].

The absence of the 1332 cm^{-1} line in the Raman spectra at a depth of 9–10 μm was an evidence of the practically complete destruction of the crystalline sp^3 phase of diamond. The appearance of the 1530 cm^{-1} band instead of the 1332 cm^{-1} line, which is associated with the sp^2 phase, was a sign of the transition of diamond to the state of amorphous carbon. The amorphized layer was not yet continuous, but consisted of islands, since at a depth of amorphization, a line at 1635 cm^{-1} from intrinsic internodes was registered. As shown in [14], Raman scattering from defects in diamond is absent when complete amorphization occurs. Due

to high sensitivity of the Raman technique to sp^2-bonded carbon structures, the absence of a wide band 1530 cm^{-1} was convincing evidence that implantation of Xe ions with the energy 167 MeV did not lead to formation of amorphous carbon for irradiation fluences less than 3.55×10^{14} cm^{-2}.

According to the intensity distribution of 400 cm^{-1} and 1230 cm^{-1} bands, amorphous sp^3-bonded carbon clusters formed along the Xe ion trajectory even at relatively low fluences. At the same time, due to the lack of detailed studies of ion-irradiated diamond with transmission electron microscopy (TEM), there is no direct evidence confirming the existence of sp^3-coupled clusters in diamond irradiated with swift heavy ions.

Figures 5a and 5b show variation in spectral position and FWHM of main Raman line 1332 cm^{-1} with Xe ion fluence. The gap between curves, plotted for the maximum fluences (the results of two independent measurements on two samples are shown), corresponded to the depth of the irradiated layer, where the 1332 cm^{-1} line was absent in the Raman spectra, but a wide band of 1530 cm^{-1} was registered. For all fluences, the low-frequency shift and FWHM of the 1332 cm^{-1} line grew monotonically with a depth up to 9.5 μm synchronously with calculated (see Fig. 2) nuclear energy losses profile. More significant electronic energy losses, as in [37], did not manifest themselves in defect formation. The same dependence was noted by all researchers of ion-irradiated diamonds (see, for example, [4,14,38–40]). It should be noted, that the depth of maximum defect formation determined experimentally from the shift and FWHM of the 1332 cm^{-1} line was approximately 1.0 μm closer to the surface than predicted by SRIM - 10.45 μm. Similar differences in the defect formation depths between calculated and experimental values in ion irradiated diamond samples were observed also in [4].

The inhomogeneous defects distribution caused elastic stresses in both the irradiated layer and the interface region with intact diamond as follows from the shift and broadening of the 1332 cm^{-1} line. An increase of ion fluence leads to monotonic increment of the spectral shift and FWHM values of the 1332 cm^{-1} line, but, in general, did not affect their depth profiles in

the irradiated layer (see Fig. 5). Change rate of the spectral shift and FWHM of main Raman line with increasing fluence was greater in the end of range region than in subsurface layer. The monotonic increment of shift and FWHM with an increase of ion fluence was interrupted after 3.55×10^{14} cm^{-2} when the change in the parameters of the 1332 cm^{-1} line seemed to be saturated. At the boundary with the incipient amorphous layer, the maximum shift of the 1332 cm^{-1} line was about 20 cm^{-1}, and its maximum broadening was about 60 cm^{-1}. In the region of projected ion range this "saturation" might be associated with the beginning of formation of carbon amorphous phase islands. Accordingly to SRIM, number vacancies for fluence 3.55×10^{14} cm^{-2} is about $2.36\cdot10^{22}$ cm^{-3} in the damage peak region, that is comparable with critical threshold of radiation damage in diamond [14,32,35,36,41]. The number of accumulated vacancies in the near-surface region for this fluence is almost 30 less and the 1332 cm^{-1} line was clearly detected, but its position and FWHM remained practically unchanged with a further accumulation of radiation damage., The maximum shift of the 1332 cm^{-1} line in subsurface region was less than 5 cm^{-1}, and its maximum broadening was about 20 cm^{-1}.

The absence of changes in the near-surface parameters distribution of the 1332 cm^{-1} line with the onset of amorphization may be due to partial relaxation of stresses in the entire irradiated layer after formation of an amorphous layer and a loss of bond integrity between the irradiated and undamaged layers in the diamond crystal lattice. Similar effects were previously described for silicon implanted with 2 MeV Xe ions [42] and 1.5 MeV Si ions [43], in which the formation of amorphous layer was accompanied by stress relaxation. One can suggest that increase in interatomic distances in the irradiated layer was not restrained by anything along the normal to the irradiated surface. Lattice swelling in direction perpendicular to the irradiated surface was observed as an additional increment in the thickness of the irradiated layer [11–14].

As known, mechanical stresses induced by the tangential expansion of the irradiated layer may result in bending even of the whole diamond plate [12,14,42]. The low-frequency

shift of the main Raman line 1332 cm^{-1}, corresponding to the expansion of the diamond crystal lattice, is linearly connected with elastic stresses [24,44–46]. According to [46] we estimated the magnitude of the elastic stresses σ in the <001> direction using relation:

$\sigma = 0.49 \cdot [GPa/cm^{-1}] \cdot \Delta\nu\ [cm^{-1}]$,

where Δν is the shift of the spectral position of the 1332 cm^{-1} line relative to that of an intact diamond sample. For instance, taking into account the above expression, the magnitude of elastic stresses for the fluence 3.55×10^{14} cm^{-2} is about 2.5 GPa in subsurface layer and about 10 GPa in damage peak region.

Figure 6 shows the behaviour of the 1332 cm^{-1} line parameters beyond the irradiated layer up to the opposite side of the diamond plate. Raman spectra were measured with a resolution of 0.25 cm^{-1} and a deepening of the excitation region on 5 μm. Spectral position (1331.9 cm^{-1}) and FWHM (1.59 cm^{-1}) for unirradiated sample are shown by a dashed line. As can be seen from Fig. 6a, the spectral position of the main Raman line beyond the irradiated layer restored nonmonotonically to its value before irradiation. For relatively small fluences (not more than 1×10^{13} cm^{-2}), the lattice expansion corresponding to the low-frequency shift of the 1332 cm^{-1} line gradually decreased with depth, reaching its original values at a depth of about 60-70 μm. Stress distribution beyond the ion range for high fluences was nearly identical: the expansion of the lattice was changed by its compression at a depth of about 3 Rp, followed by an increase in compression stresses up to 6–7 Rp. Further, with increasing depth, compression stresses monotonously weakened, but did not reach the value before irradiation even on the opposite side of the plate (at a depth of about 800 μm).

As follows from Figure 6, the unirradiated part of the diamond plate “restrained” the expansion of the crystal lattice in the irradiated layer. With this in mind, it is expected that the stress distribution in diamonds irradiated with swift heavy ions will depend on the thickness of the plates.

Conclusions

Accumulation of radiation damage and associated mechanical stresses in diamond samples irradiated by 167 MeV Xe ions were studied with Raman spectroscopy. The main Raman line 1332 cm^{-1} became less intense, broadened and shifted to lower frequencies region due to radiation damage of the diamond lattice. Stress distribution profiles in irradiated layer and beyond it were derived from spectral position of the 1332 cm^{-1} line. The expansion of the lattice in the irradiated by 167 MeV Xe ions, 10 μm layer leads to appearing tangential stresses that cause deformation (bending) of the entire diamond wafer. The undamaged part of the diamond lattice is under alternating tensile and compressive stresses that "compensate" for the expansion of the lattice in the irradiated layer. Partial relaxation of mechanical stresses was observed in the entire irradiated layer, indicating its lower hardness and associated with the onset of amorphization in the region of maximum defect concentration.

References:

[1] R. Kalish, A. Reznik, S. Prawer, D. Saada, J. Adler, Ion-Implantation-Induced Defects in Diamond and Their Annealing: Experiment and Simulation, Phys. Status Solidi. 174 (1999) 83–99. https://doi.org/10.1002/(SICI)1521-396X(199907)174:1<83::AID-PSSA83>3.0.CO;2-3.

[2] A.M. Zaitsev, Optical properties of diamond : a data handbook, Springer, 2001.

[3] S. Prawer, K.W. Nugent, D.N. Jamieson, The Raman spectrum of amorphous diamond, Diam. Relat. Mater. 7 (1998) 106–110. https://doi.org/10.1016/S0925-9635(97)00194-5.

[4] J.O. Orwa, K.W. Nugent, D.N. Jamieson, S. Prawer, Raman investigation of damage caused by deep ion implantation in diamond, Phys. Rev. B - Condens. Matter Mater. Phys. 62 (2000) 5461–5472. https://doi.org/10.1103/PhysRevB.62.5461.

[5] R. Brunetto, G.A. Baratta, G. Strazzulla, Amorphization of diamond by ion irradiation: a Raman study, J. Phys. Conf. Ser. 6 (2005) 120–125. https://doi.org/10.1088/1742-6596/6/1/011.

[6] I.A. Dobrinets, V.G. Vins, A.M. Zaitsev, HPHT-Treated Diamonds, in: Diam. Forever, 2013: pp. 5–25. https://doi.org/10.1007/978-3-642-37490-6.

[7] A.M. Zaitsev, High energy ion implantation into diamond and cubic boron nitride, Nucl. Inst. Methods Phys. Res. B. 62 (1991) 81–98. https://doi.org/10.1016/0168-583X(91)95933-5.

[8] J.F. Prins, T.E. Derry, J.P.F. Sellschop, Volume expansion of diamond during ion implantation, Phys. Rev. B. 34 (1986) 8870–8874. https://doi.org/10.1103/PhysRevB.34.8870.

[9] V.D. Vankar, N. Dilawar, Ion irradiation effects in diamond and diamond like carbon thin films, Vacuum. 47 (1996) 1275–1280. https://doi.org/10.1016/S0042-207X(96)00169-8.

[10] V.A. Nikolaenko, E.A. Krasikov, Effect of reactor radiation intensity on crystal lattice expansion in diamond, At. Energy. 115 (2014) 267–276. https://doi.org/10.1007/s10512-014-9782-7.

[11] F. Bosia, N. Argiolas, M. Bazzan, B.A. Fairchild, A.D. Greentree, D.W.M. Lau, P. Olivero, F. Picollo, S. Rubanov, S. Prawer, Direct measurement and modelling of internal strains in ion-implanted diamond, J. Phys. Condens. Matter. 25 (2013). https://doi.org/10.1088/0953-8984/25/38/385403.

[12] R.A. Khmelnitsky, V.A. Dravin, A.A. Tal, M.I. Latushko, A.A. Khomich, A. V. Khomich, A.S. Trushin, A.A. Alekseev, S.A. Terentiev, Mechanical stresses and amorphization of ion-implanted diamond, Nucl. Instruments Methods Phys. Res. Sect. B Beam Interact. with Mater. Atoms. 304 (2013) 5–10. https://doi.org/10.1016/j.nimb.2013.03.030.

[13] M. Piccardo, F. Bosia, P. Olivero, N. Pugno, An analytical model for the mechanical deformation of locally graphitized diamond, Diam. Relat. Mater. 48 (2014) 73–81. https://doi.org/10.1016/j.diamond.2014.07.006.

[14] R.A. Khmelnitsky, V.A. Dravin, A.A. Tal, E. V. Zavedeev, A.A. Khomich, A. V. Khomich, A.A. Alekseev, S.A. Terentiev, Damage accumulation in diamond during ion implantation, J. Mater. Res. 30 (2015) 1583–1592. https://doi.org/10.1557/jmr.2015.21.

[15] A.M. Zaitsev, Luminescence of Ion-Implanted Diamond and Cubic Boron Nitride, Dr. Sc, University of Minsk, 1992.

[16] N.M. Kazyuchits, A. V. Konovalova, I.I. Azarko, F.F. Yakotsuk, I.N. Bogdanov, Y.K. Kabak, Effect of synthesis conditions on the impurity composition of STM Almazot diamond single crystals, Inorg. Mater. 50 (2014) 130–135.

[17] Gikal B.N. et al., Cyclotron Based Complex IC-100 for Scientific and Applied Research, Phys. Part. Nucl. 5 (2008) 59-85 (in Russian).

[18] J.F. Ziegler, J.P. Biersack, The Stopping and Ranges of Ions in Solids, Pergamon Press,

New York, 1985.

[19] James Ziegler - SRIM & TRIM, (n.d.). http://www.srim.org/ (accessed November 15, 2019).

[20] D. Kirillov, G.J. Reynolds, Linewidths of phonon lines of natural and synthetic diamonds, Appl. Phys. Lett. 65 (1994) 1641–1643. https://doi.org/10.1063/1.112936.

[21] N. V Surovtsev, I.N. Kupriyanov, Effect of Nitrogen Impurities on the Raman Line Width in Diamond, Revisited, J. Phys. Condens. Matter. 11 (1999) 4767–4774. https://doi.org/10.3390/cryst7080239.

[22] T. Bauer, M. Schreck, H. Sternschulte, B. Stritzker, High growth rate homoepitaxial diamond deposition on off-axis substrates, in: Diam. Relat. Mater., 2005: pp. 266–271. https://doi.org/10.1016/j.diamond.2004.10.043.

[23] M. Muehle, M.K. Yaran, M.F. Becker, T. Schuelke, J. Asmussen, Y. Gu, D.K. Reinhard, T.A. Grotjohn, Quality and internal stress of single crystalline diamond synthesized by microwave plasma assisted chemical vapor deposition, in: 2012.

[24] S. Prawer, R.J. Nemanich, Raman spectroscopy of diamond and doped diamond, Philos. Trans. R. Soc. London. Ser. A Math. Phys. Eng. Sci. 362 (2004) 2537–2565. https://doi.org/10.1098/rsta.2004.1451.

[25] O.N. Poklonskaya, A.A. Khomich, Raman scattering in a diamond crystal implanted by high-energy nickel ions, J. Appl. Spectrosc. 80 (2013) 715–720. https://doi.org/10.1007/s10812-013-9831-3.

[26] O.N. Poklonskaya, S.A. Vyrko, A.A. Khomich, A.A. Averin, A. V. Khomich, R.A. Khmelnitsky, N.A. Poklonskia, Raman Scattering in Natural Diamond Crystals Implanted with High-Energy Ions and Irradiated with Fast Neutrons, J. Appl. Spectrosc. 81 (2015) 969–977. https://doi.org/10.1007/s10812-015-0037-8.

[27] A. V. Khomich, R.A. Khmelnitskii, X.J. Hu, A.A. Khomich, A.F. Popovich, I.I. Vlasov, V.A. Dravin, Y.G. Chen, A.E. Karkin, V.G. Ralchenko, Radiation damage effects on

optical, electrical, and thermophysical properties of cvd diamond films, J. Appl. Spectrosc. 80 (2013) 707–714. https://doi.org/10.1007/s10812-013-9830-4.

[28] J.D. Hunn, S.P. Withrow, C.W. White, D.M. Hembree, Raman scattering from MeV-ion implanted diamond, Phys. Rev. B. 52 (1995) 8106–8111. https://doi.org/10.1103/PhysRevB.52.8106.

[29] E.H. Lee, D.M. Hembree, G.R. Rao, L.K. Mansur, Raman scattering from ion-implanted diamond, graphite, and polymers, Phys. Rev. B. 48 (1993) 15540–15551. https://doi.org/10.1103/PhysRevB.48.15540.

[30] F. Fontaine, A. Deneuville, E. Gheeraert, P. Gonon, L. Abello, G. Lucazeau, Reality of doping by boron implantation of CVD polycrystalline diamond from a comparison of Raman and electrical measurements, Diam. Relat. Mater. 3 (1994) 623–627. https://doi.org/10.1016/0925-9635(94)90237-2.

[31] H. Amekura, N. Kishimoto, Effects of high-fluence ion implantation on colorless diamond self-standing films, J. Appl. Phys. 104 (2008). https://doi.org/10.1063/1.2978215.

[32] C. Uzan-Saguy, C. Cytermann, R. Brener, V. Richter, M. Shaanan, R. Kalish, Damage threshold for ion-beam induced graphitization of diamond, Appl. Phys. Lett. 67 (1995) 1194–1196. https://doi.org/10.1063/1.115004.

[33] G. Strazzulla, G.A. Baratta, F. Spinella, Production and evolution of carbonaceous material by ion irradiation in space, Adv. Sp. Res. 15 (1995) 385–399. https://doi.org/10.1016/S0273-1177(99)80109-4.

[34] G.A. Baratta, V. Mennella, J.R. Brucato, L. Colangeli, G. Leto, M.E. Palumbo, G. Strazzulla, Raman spectroscopy of ion-irradiated interplanetary carbon dust analogues, J. Raman Spectrosc. 35 (2004) 487–496. https://doi.org/10.1002/jrs.1169.

[35] R. Brunetto, G.A. Baratta, G. Strazzulla, Raman spectroscopy of ion irradiated diamond, J. Appl. Phys. 96 (2004) 380–386. https://doi.org/10.1063/1.1759080.

[36] D.P. Hickey, K.S. Jones, R.G. Elliman, Amorphization and graphitization of single-crystal diamond - A transmission electron microscopy study, Diam. Relat. Mater. 18 (2009) 1353–1359. https://doi.org/10.1016/j.diamond.2009.08.012.

[37] G. García, M. Díaz-Híjar, V. Tormo-Márquez, I. Preda, O. Peña-Rodríguez, J. Olivares, Structural damage on single-crystal diamond by swift heavy ion irradiation, Diam. Relat. Mater. 58 (2015) 226–229. https://doi.org/10.1016/j.diamond.2015.08.014.

[38] D.N. Jamieson, S. Prawer, K.W. Nugent, S.P. Dooley, Cross-sectional Raman microscopy of MeV implanted diamond, Nucl. Inst. Methods Phys. Res. B. 106 (1995) 641–645. https://doi.org/10.1016/0168-583X(96)80036-X.

[39] L. Nasdala, D. Grambole, M. Wildner, A.M. Gigler, T. Hainschwang, A.M. Zaitsev, J.W. Harris, J. Milledge, D.J. Schulze, W. Hofmeister, W.A. Balmer, Radio-colouration of diamond: A spectroscopic study, Contrib. to Mineral. Petrol. 165 (2013) 843–861. https://doi.org/10.1007/s00410-012-0838-1.

[40] F. Agulló-Rueda, N. Gordillo, M.D. Ynsa, A. Maira, J. Cañas, M.A. Ramos, Lattice damage in 9-MeV-carbon irradiated diamond and its recovery after annealing, Carbon N. Y. 123 (2017) 334–343. https://doi.org/10.1016/j.carbon.2017.07.076.

[41] B.A. Fairchild, S. Rubanov, D.W.M. Lau, M. Robinson, I. Suarez-Martinez, N. Marks, A.D. Greentree, D. McCulloch, S. Prawer, Mechanism for the Amorphisation of Diamond, Adv. Mater. 24 (2012) 2024–2029. https://doi.org/10.1002/adma.201104511.

[42] C.A. Volkert, Stress and plastic flow in silicon during amorphization by ion bombardment, J. Appl. Phys. 70 (1991) 3521–3527. https://doi.org/10.1063/1.349247.

[43] X. Huang, F. Ninio, L.J. Brown, S. Prawer, Raman scattering studies of surface modification in 1.5 MeV Si-implanted silicon, J. Appl. Phys. 77 (1995) 5910–5915. https://doi.org/10.1063/1.359171.

[44] M.H. Grimsditch, E. Anastassakis, M. Cardona, Effect of uniaxial stress on the zone-center optical phonon of diamond, Phys. Rev. B. 18 (1978) 901–904.

https://doi.org/10.1103/PhysRevB.18.901.

[45] J.W. Ager, M.D. Drory, Quantitative measurement of residual biaxial stress by Raman spectroscopy in diamond grown on a Ti alloy by chemical vapor deposition, Phys. Rev. B. 48 (1993) 2601–2607. https://doi.org/10.1103/PhysRevB.48.2601.

[46] F. Ahmed, K. Durst, S. Rosiwal, J. Fandrey, J. Schaufler, M. Göken, In-situ tensile testing of crystalline diamond coatings using Raman spectroscopy, Surf. Coatings Technol. 204 (2009) 1022–1025. https://doi.org/10.1016/j.surfcoat.2009.04.030.

Figure captions:

Fig. 1. Schematic view of the Raman analysis measurements (a) and a photo of a polished cross-section of the diamond plate for the fluence 8.15×10^{14} cm^{-2} (b).

Fig. 2. Energy loss profiles, primary carbon vacancies and implanted impurity distributions for Xe ions with the energy 167 MeV. Results of calculations are given for the fluence 1 cm^{-2}.

Fig. 3. Raman/PL spectra evolution in the near surface layer (z = 1.5 μm) with increasing irradiation fluence of Xe ions with the energy 167 MeV. Values of fluence [ions/cm^2] are indicated in labels to curves. Spectra are shown without displacement along the ordinate axis.

Fig.4. Raman/PL spectra evolution with the irradiated layer depth for ion fluences (a) 6.1×10^{12} cm^{-2} and (b) 8.15×10^{14} cm^{-2}. Spectra are shown without displacement along the ordinate axis.

Fig. 5. Depth profile of (a) spectral position and (b) FWHM of the 1332cm^{-1} Raman line in diamond samples irradiated with 167MeV Xe ions for different ion fluences.

Fig. 6. FWHM (a) and spectral position (b) depth profiles of 1332 cm^{-1} line beyond the ion range in diamond plate irradiated with 167MeV Xe ions for different ion fluences. Dashed line corresponds to virgin diamond sample.

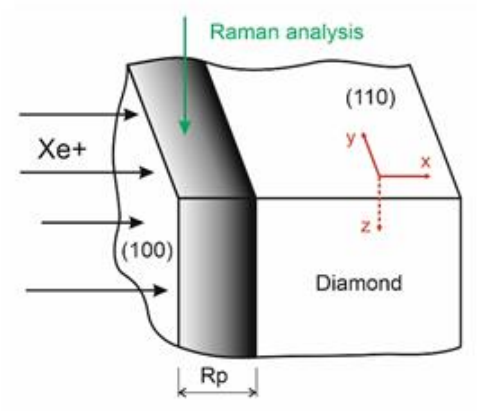

(a)

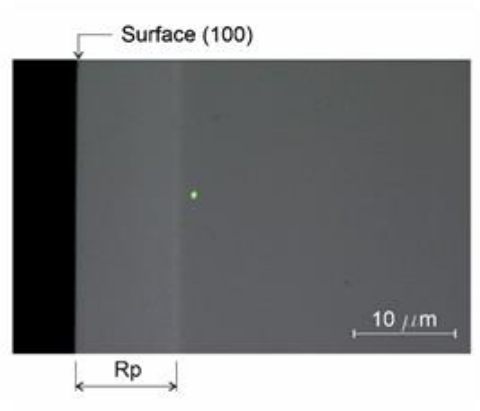

(b)

1

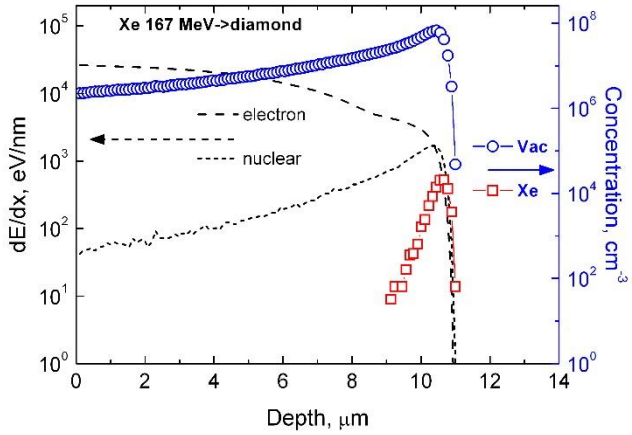
Xe 167 MeV->diamond
electron
nuclear
Vac
Xe
dE/dx, eV/nm
Concentration, cm-3
Depth, μm

2

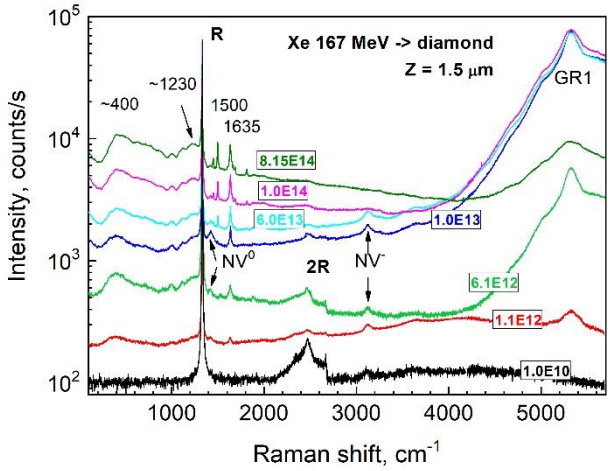
Xe 167 MeV -> diamond
Z = 1.5 μm
R
~400
~1230
1500
1635
GR1
8.15E14
1.0E14
6.0E13
1.0E13
NV0
2R
NV-
6.1E12
1.1E12
1.0E10
Intensity, counts/s
Raman shift, cm-1

3

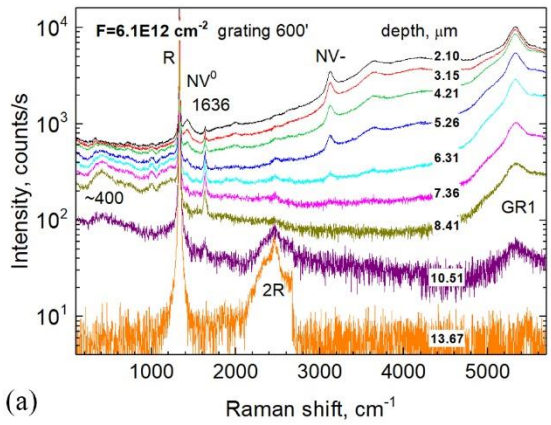
F=6.1E12 cm-2 grating 600'
depth, μm
R
NV0
1636
NV-
2.10
3.15
4.21
5.26
6.31
7.36
8.41
10.51
13.67
~400
GR1
2R
Intensity, counts/s
Raman shift, cm-1

(a)

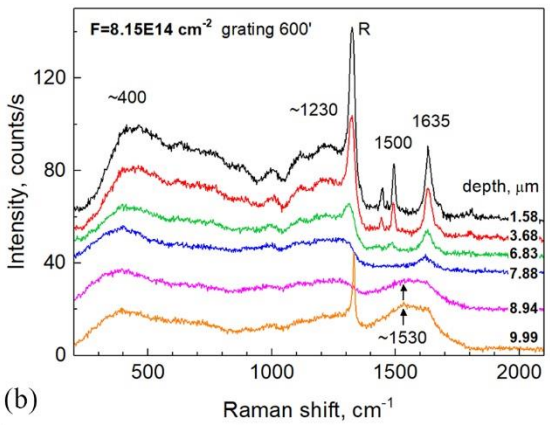
F=8.15E14 cm-2 grating 600'
R
~400
~1230
1500
1635
depth, μm
1.58
3.68
6.83
7.88
8.94
9.99
~1530
Intensity, counts/s
Raman shift, cm-1

(b)

4

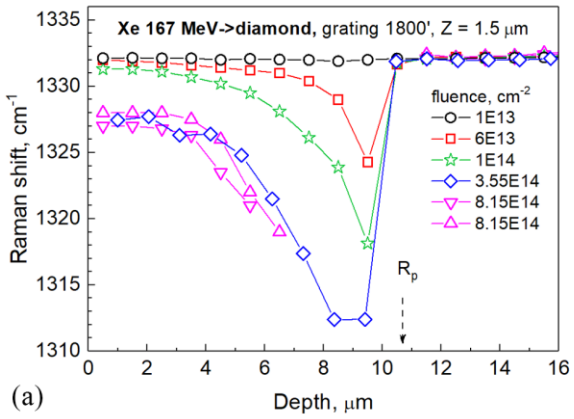
Xe 167 MeV->diamond, grating 1800', Z = 1.5 μm
Raman shift, cm-1
Depth, μm
fluence, cm-2
1E13
6E13
1E14
3.55E14
8.15E14
8.15E14
Rp

(a)

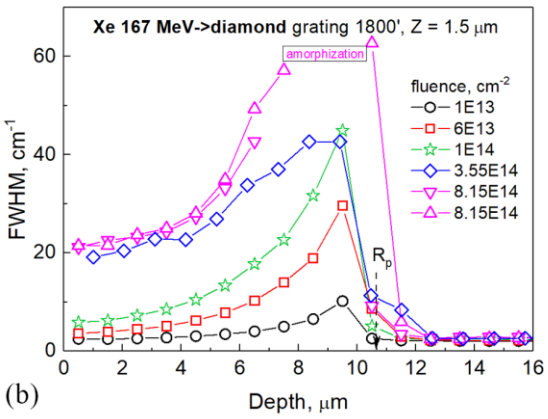
Xe 167 MeV->diamond grating 1800', Z = 1.5 μm
amorphization
FWHM, cm-1
Depth, μm
fluence, cm-2
1E13
6E13
1E14
3.55E14
8.15E14
8.15E14
Rp

(b)

5

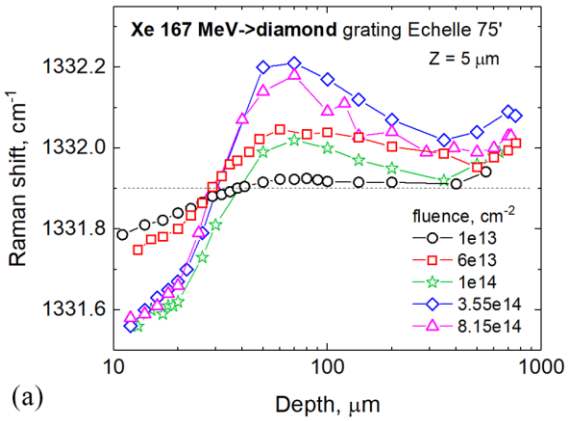
Xe 167 MeV->diamond grating Echelle 75'
Z = 5 μm
Raman shift, cm-1
1332.2
1332.0
1331.8
1331.6
10
100
1000
Depth, μm
fluence, cm-2
1e13
6e13
1e14
3.55e14
8.15e14

(a)

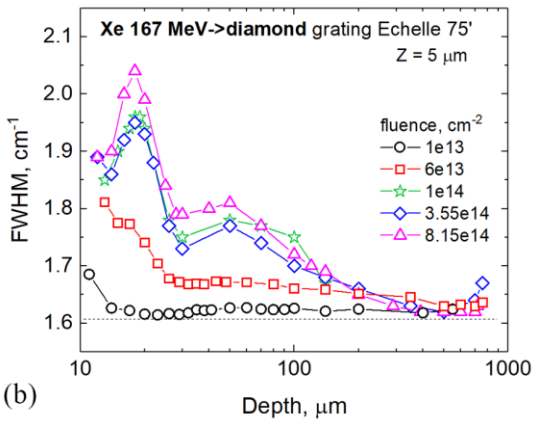
Xe 167 MeV->diamond grating Echelle 75'
Z = 5 μm
FWHM, cm-1
2.1
2.0
1.9
1.8
1.7
1.6
10
100
1000
Depth, μm
fluence, cm-2
1e13
6e13
1e14
3.55e14
8.15e14

(b)